Proc. Natl. Acad. Sci. USA
Vol. 91, pp. 3388–3392, April 1994
Medical Sciences

Three-dimensional spectral–spatial EPR imaging of free radicals in the heart: A technique for imaging tissue metabolism and oxygenation

(aorta/oximetry)

PERIANNAN KUPPUSAMY, MICHAEL CHZHAN, KAMAL VIJ, MICHAEL SHTEYNBUK, DAVID J. LEFER, ELIANA GIANNELLA, AND JAY L. ZWEIER

The EPR Laboratories and Department of Medicine, The Johns Hopkins University School of Medicine, Francis Scott Key Medical Center, 5501 Hopkins Bayview Circle, Baltimore, MD 21224

Communicated by William A. Hagins, December 10, 1993

ABSTRACT **It has been hypothesized that free radical metabolism and oxygenation in living organs and tissues such as the heart may vary over the spatially defined tissue structure. In an effort to study these spatially defined differences, we have developed electron paramagnetic resonance imaging instrumentation enabling the performance of three-dimensional spectral–spatial images of free radicals infused into the heart and large vessels. Using this instrumentation, high-quality three-dimensional spectral–spatial images of isolated perfused rat hearts and rabbit aortas are obtained. In the isolated aorta, it is shown that spatially and spectrally accurate images of the vessel lumen and wall could be obtained in this living vascular tissue. In the isolated rat heart, imaging experiments were performed to determine the kinetics of radical clearance at different spatial locations within the heart during myocardial ischemia. The kinetic data show the existence of regional and transmural differences in myocardial free radical clearance. It is further demonstrated that EPR imaging can be used to noninvasively measure spatially localized oxygen concentrations in the heart. Thus, the technique of spectral–spatial EPR imaging is shown to be a powerful tool in providing spatial information regarding the free radical distribution, metabolism, and tissue oxygenation in living biological organs and tissues.**

Electron paramagnetic resonance (EPR) spectroscopy has been widely applied to study free radicals and paramagnetic metal ions in chemical and biological systems. It is the direct and definitive technique for measuring and characterizing molecules with unpaired electron spin. However, EPR studies of biological organs or tissues have been hampered by the lossy nature of these samples and the need for specially designed resonators to accommodate these large samples. Over the last decade EPR has been widely applied to measure the mechanisms of free radical generation in isolated cells and tissues. Recently, instruments have been developed that enable noninvasive *in vivo* EPR measurements of free radicals in whole animals and functioning whole organs (1–5). These instruments have generally utilized low-frequency microwaves of 1–2 GHz or below to enable tissue penetration. In addition, lumped circuit resonator technology has enabled optimization of sensitivity for *in vivo* applications.

Free radicals have been suggested to be key mediators of the injury that occurs upon reperfusion of the ischemic heart (6, 7). It has also been suggested that ischemia may alter the ability of the heart to metabolize reactive oxygen free radicals. There are also fundamental questions regarding oxygen metabolism in the heart and its role in regulating contractile function and energy metabolism. In addition, there are questions regarding the presence of spatially defined alterations in cellular metabolism in the heart and large arterial vessels. In the heart, the endocardium, the inner layer of the cardiac chambers, is more sensitive to ischemic injury than the epicardium, and it has been hypothesized that there may be transmural variations in myocardial oxygenation and metabolism (8, 9). However, there has been no previous technique that could determine if these transmural variations exist. In large arterial vessels it has been shown that occlusion with a lack of flow results in injury with altered vascular reactivity (8, 9). This injury has been difficult to explain since it occurs in the face of normal intra-arterial oxygen tensions, and it has not been previously possible to measure transmural metabolism and the transmural concentrations of oxygen in these vessels. Thus, there has been a great need for a technique capable of measuring the spatial distribution of free radicals and oxygen in organs and tissues such as the heart and large vessels.

EPR spectroscopy can be applied to obtain spatial information by utilizing magnetic field gradients (10), in a manner similar to that of NMR imaging. EPR imaging, however, is faced with a number of technical problems, which make this technique more difficult to achieve in practice than that of NMR. The linewidths of EPR signals are 3 orders of magnitude larger than those of NMR signals, and hence EPR imaging requires 100–1000 times more powerful gradients. The paramagnetic centers to be studied are present in submillimolar concentrations compared to more than 100 M concentrations of water protons utilized in NMR imaging. Since spectral information is required to characterize the properties and structure of free radicals, as well as to perform oximetry measurements, spectral–spatial imaging must be performed to address the important problems discussed above.

Over the last decade, EPR imaging experiments have been performed by a number of groups around the world on a variety of samples (10–21). With biological organs and living samples, these studies, in general, have provided only low-resolution spatial images or one-dimensional spectral–one-dimensional spatial images of free radicals. Recently methods have been developed enabling localized EPR spectroscopy by implanting oxygen-sensitive paramagnetic probes (22). To perform oximetry studies on asymmetric biological samples, such as the heart, using imaging, it is necessary to include a spectral dimension along with two or three spatial dimensions. The experiment must be performed and the image must

The publication costs of this article were defrayed in part by page charge payment. This article must therefore be hereby marked "*advertisement*" in accordance with 18 U.S.C. §1734 solely to indicate this fact.

Abbreviations: 2D, two dimensional; 3D, three dimensional; PC, personal computer; GPIB, general purpose interface bus; TEMPO, 2,2,6,6-tetramethylpiperidine-1-oxyl; PDT, 4-oxo-2,2,6,6-tetramethylpiperidine-d_{16}-1-oxyl.

be obtained on a fast time scale so as to capture the temporal variations in radical metabolism or oxygen consumption. In addition, reasonably good submillimeter image resolution must be obtained in order to make meaningful interpretations.

In view of the important cardiovascular pathophysiologic questions that cannot be addressed with other existing techniques, we have developed instrumentation enabling the performance of three-dimensional (3D) spectral–spatial EPR images of the heart and large vessels. This instrumentation is applied to obtain images of free radical metabolism and oxygen concentrations in the heart. Assessment of regional and transmural differences in vascular and myocardial free radical metabolism and oxygenation are performed.

METHODS

L-Band Resonator and Spectrometer. EPR spectra were recorded using an L-band bridge similar in design to that described previously (4). A new ceramic three-loop two-gap reentrant resonator design was developed to enable the high sensitivity and high stability required for EPR imaging (23). This resonator design has the advantage over previous single-loop, loop-gap designs (4), in that its thickness is much less and can be made almost as thin as the sample. This is particularly important for EPR imaging where two or three sets of powerful water-cooled gradient coils must be accommodated, in addition to the sample, sample cavity, and modulation coils. The resonator dimensions were as follows: radius, 10 mm; capacitive plate length, 6 mm; capacitive plate width, 17 mm; and capacitive gap, 0.23 mm (23). This resonator provides a relatively selective slice of maximum H_1 field. The resonant frequency was 1.319 GHz with an unloaded Q factor of 2930.

EPR measurements were performed using a Bruker signal channel (ER 023M) and field controller (ER 032M) interfaced to a personal computer (PC). The microwave frequency was measured over the general purpose interface bus (GPIB) using an EIP 975 microwave counter.

Gradient Coils. EPR imaging measurements were performed using a modified Varian XL-100 NMR magnet in which the pole faces were remachined to a gap of 4.5 inches and appropriate ring shims were placed to achieve an optimized homogeneity of better than 1 part in 10^5 over a sample volume of 1 cm^3 at the center of the gap.

Three sets of water-cooled gradient coil assemblies were attached to the pole faces of the magnet. A modified Helmholtz pair was used to generate the gradient along the z axis (the direction of the static magnetic field), and two sets of pair coils were used to generate the x and y gradients. Each set was capable of generating sustained field gradients of at least 150 G/cm. Each set of coils was independently powered with a Hewlett-Packard power supply (model 6030A), interfaced to the PC via GPIB bus.

Data Acquisition and Image Reconstruction. Projection data acquisition and subsequent image reconstruction were performed using a 486-based PC equipped with an IEEE-488 GPIB board. Software capable of 3D spectral–spatial data acquisition, reduction, image reconstruction, image analysis, and simulation was developed. The PC was programmed to control the signal channel, field controller, and the gradient power supplies (Fig. 1). The software controlled the three gradients, enabling the user to select any arbitrary spatial plane of interest for image acquisition and reconstruction.

Projection data was then collected for N orientations in the spatial–spatial plane and N orientations in the spectral–spatial plane for each spatial–spatial orientation, thus for a total of $N \times N$ orientations for each image. The N projections in a plane were obtained over 180° with equal angular

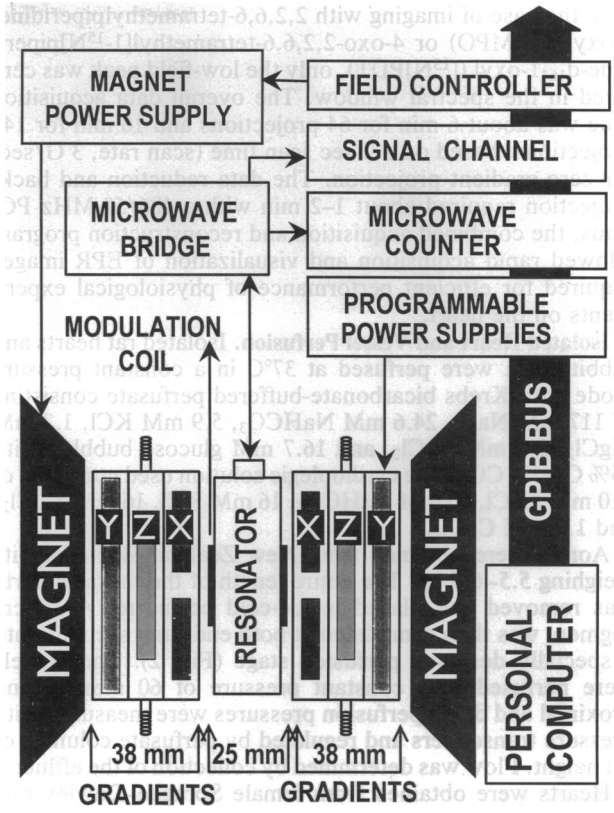

FIG. 1. Block diagram of EPR imaging instrument.

increments. For each projection, the magnitude of the gradient, G, for a projection angle α, was calculated as [24]

$$G = (\Delta H/\Delta X)\tan(\alpha), \quad [1]$$

where ΔH and ΔX are the values of spectral and spatial windows defining the pseudo-plane from which data are acquired. The scan range was varied from the base value ΔH according to the relationship [24]:

$$\text{scan range} = \Delta H/\cos(\alpha). \quad [2]$$

The scan time for each projection data collection was kept proportional to the scan range, such that the resultant sweep rate (gauss/second) was constant. Projections involving relatively large gradients, and hence longer scan times or larger scan ranges, were measured with increased receiver gain and time constant, and the data was normalized accordingly for base value (zero-gradient) settings. The microwave frequency was measured at the end of each projection and used to correct any shift in the projection due to drift in the frequency. A delay time of 500 msec was given between acquisitions to allow stabilization of each new gradient field. Where required, the order of projections was scrambled to minimize heating of the gradient coils.

A total of 256 points per projection were collected by integrative digitization of the analog output from the signal channel. During data reduction, the 256 points were subsampled to 64 points and normalized for constant intensity (24). The data was then integrated, baseline corrected, and smoothed using a Gaussian filter, all in the Fourier space. A three-point (second difference) filter was then applied to the data. A two-stage backprojection algorithm was used to reconstruct the image of the object (25). The first stage produced N pseudo two-dimensional (2D) spectral–spatial image slices ($N \times 64 \times 64$), while the second stage produced the 3D spectral–spatial–spatial image ($64 \times 64 \times 64$).

In the case of imaging with 2,2,6,6-tetramethylpiperidine-1-oxyl (TEMPO) or 4-oxo-2,2,6,6-tetramethyl[1-^{15}N]piperidine-d_{16}-1-oxyl ([^{15}N]PDT), only the low-field peak was centered in the spectral window. The overall data acquisition time was about 6 min for 64 projections and 16 min for 144 projections, based on a 2-sec scan time (scan rate, 3 G/sec) for zero-gradient projection. The data reduction and back-projection required about 1–2 min with a 486/50-MHz PC. Thus, the combined acquisition and reconstruction program allowed rapid acquisition and visualization of EPR images required for efficient performance of physiological experiments on the heart.

Isolated Heart and Vessel Perfusion. Isolated rat hearts and rabbit aorta were perfused at 37°C in a constant pressure mode with Krebs bicarbonate-buffered perfusate consisting of 117 mM NaCl, 24.6 mM $NaHCO_3$, 5.9 mM KCl, 1.2 mM $MgCl_2$, 2.0 mM $CaCl_2$, and 16.7 mM glucose bubbled with 95% O_2/5% CO_2. The cardioplegic solution used consisted of 110 mM NaCl, 10 mM $NaHCO_3$, 16 mM KCl, 16 mM $MgCl_2$, and 1.2 mM $CaCl_2$.

Aortas were obtained from New Zealand White rabbits weighing 5.5–6.5 kg. The entire length of the thoracic aorta was removed and placed in ice-cold perfusate. A 3.0-cm segment was then cannulated at both ends and secured onto a specially designed perfusion stage (Fig. 2). The vessels were perfused at a constant pressure of 60 mmHg, and proximal and distal perfusion pressures were measured with pressure transducers and regulated by perfusate columns of set height. Flow was determined by collection of the effluent.

Hearts were obtained from female Sprague–Dawley rats (300–400 g) and perfused retrogradely with a constant pressure of 80 mmHg by the method of Langendorff. A fluid-filled balloon was placed within the left ventricle and connected via a hydraulic line to a pressure transducer to enable continuous measurement of contractile function (4) (Fig. 2). Spin-label concentrations of 0.5 mM or 1.0 mM were used, which were sufficiently low as to produce no alterations in contractile function and negligable concentration-dependent broadening of the EPR signal.

RESULTS

Imaging of Phantoms. To check the quality of spectral–spatial data obtained on large lossy aqueous samples, phantoms were constructed consisting of either single or concentric tubes containing free radical solutions of TEMPO or [^{15}N]PDT. 3D spectral spatial imaging of a 9-mm i.d. tube containing an aqueous solution of 0.5 mM [^{15}N]PDT was performed perpendicular to the longitudinal axis of the tube. As shown in Fig. 3*A*, a solid uniform disk was obtained. The spatial dimension measured from the image was in good agreement with the sample size. The spectral data of the image showed a uniform linewidth of 1.5 G (peak-to-peak width of the derivative line) over the entire sample. Fig. 3*B* shows the free radical image of a ring phantom of a 1 mM aqueous TEMPO solution filled in the annular space between two concentric tubes of 14 mm (i.d.) and 10 mm (o.d.). The spectral data of the image showed a uniform linewidth of 1.7 G.

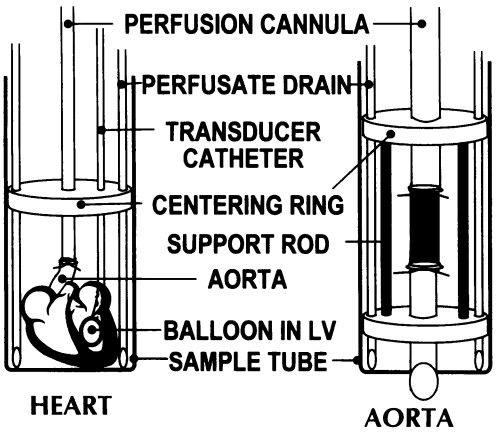

FIG. 2. Diagram of isolated rat heart and rabbit aorta preparation used for EPR imaging experiment.

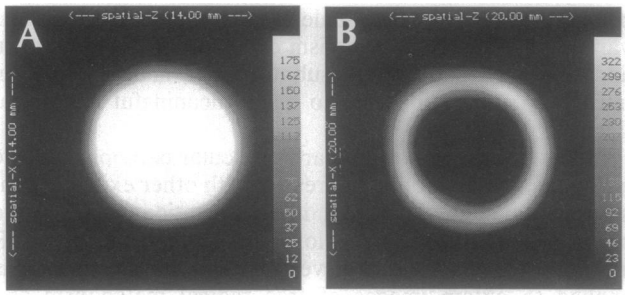

FIG. 3. 3D spectral–spatial EPR image of phantoms. (*A*) 2D spatial cross-sectional (14 × 14 mm^2) EPR intensity image of a 9-mm (i.d.) cylindrical tube containing 0.5 mM aqueous [^{15}N]PDT (projections, 256; spectral window, 8.0 G; spatial window, 14 mm; maximum gradient, 57.7 G/cm). (*B*) 2D spatial cross-sectional (20 × 20 mm^2) image of EPR intensity of 1 mM TEMPO ring (14-mm o.d, 10-mm i.d.) phantom (projections, 64; spectral window, 6.0 G; spatial window, 20 mm; maximum gradient, 24.65 Gauss/cm).

Imaging of the Aorta. The isolated perfused rabbit aorta preparation was studied as described above. Control EPR spectra were recorded, and then an infusion of the TEMPO free radical was started with a concentration of 1.0 mM in the perfusate solution. Serial 10-sec zero-gradient EPR spectra were obtained to monitor the development of the TEMPO signal. After about 10 min of infusion, a steady-state magnitude of the EPR signal intensity was reached. With the perfusion continued, 3D spectral–spatial EPR images were acquired. A total of 64 projections were acquired in 12 min with a base projection acquisition time of 4 sec. Fig. 4*A* shows the spatial map of TEMPO signal intensity projected across the longitudinal axis of the aorta. Subsequently, the aorta was perfused with perfusate containing 40 mM ferricyanide, a paramagnetic contrast agent. After steady state was reached with ferricyanide, the image acquisition was repeated. As can be seen from Fig. 4*B*, in the presence of ferricyanide, the signal arising from the radical pool within the lumen of the vessel was greatly attenuated and the vessel wall could be clearly seen.

Imaging of the Heart. Hearts were infused with TEMPO for 10 min to reach steady state, and EPR acquisitions of 64 or 144 projections were performed every 12 or 16 min, respectively. A series of 10 images was obtained from the loaded heart. These images corresponded well with cross-sectional

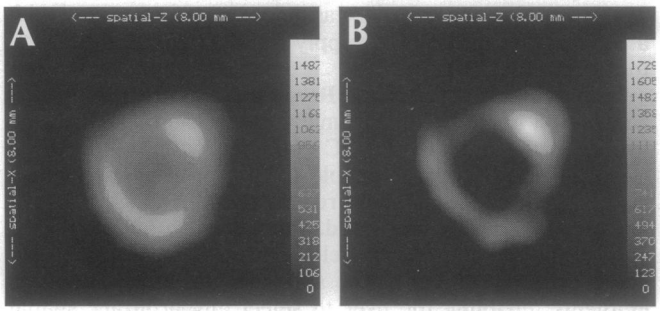

FIG. 4. EPR images (8 × 8 mm^2) rabbit aorta obtained from a 3D spectral–spatial data reconstructed from 64 projections. (*A*) Aorta perfused with 1.0 mM TEMPO. (*B*) Aorta perfused with 1.0 mM TEMPO and 40 mM ferricyanide. The data acquisition parameters were as follows: acquisition time, 12 min; spectral window, 7.0 G; spatial window, 8 mm; maximum gradient, 49.3 G/cm.

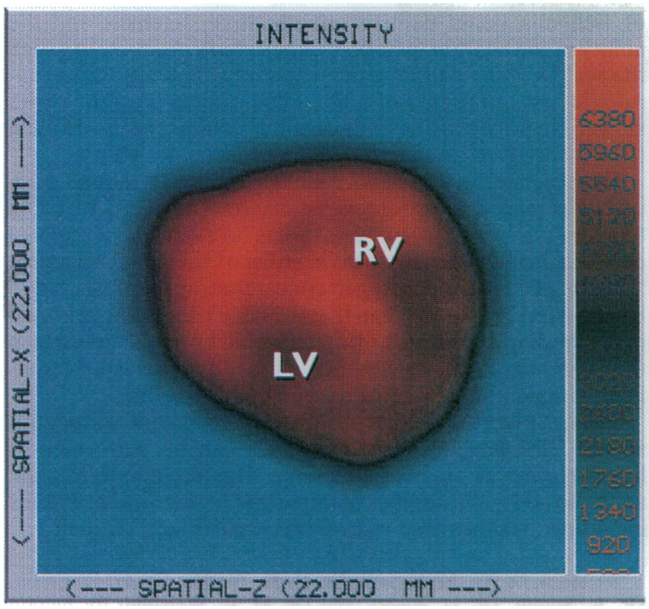

FIG. 5. Cross-sectional transverse 2D spatial EPR image (22 × 22 mm^2) of the rat heart obtained from a 3D spectral–spatial data reconstructed from 144 projections. The intensity data was obtained by selective integration of spectral slices 20–44. The structure of the left ventricle (LV) and right ventricle (RV) are observed in the EPR image to be similar to that of a short axis histologic tissue slice. The data acquisition parameters were as follows: acquisition time, 16 min; spectral window, 8.0 G; spatial window, 22 mm; maximum gradient, 27.4 G/cm.

short axis sections through the rat heart as would have been expected from the orientation of the heart in the center of the resonator. The left ventricular cavity, right ventricular cavity, and left ventricular and right ventricular myocardium were visualized (Fig. 5). In another heart after loading and acquisition of two control images, the heart was cardiopleged and subjected to a global ischemia at 24°C. During cardioplegia, a series of four additional images were obtained followed by two images during reperfusion (Fig. 6). The intensity of the images decreased as a function of duration of ischemia as the radical label was metabolized. The label cleared more rapidly from the outer myocardial walls (epicardium) than from the endocardium or from the center of the left ventricle. The epicardial contour corresponded to the outer rim of the image. The endocardial contour was defined as the dark circle at the center of the image and corresponded to the site of the balloon placed in the left ventricle. The balloon contained a volume of 0.2 ml and had a diameter of ≈5 mm, which served to confirm the endocardial location. At four selected regions, 12, 3, 6, and 9 o'clock positions, the kinetics of radical clearance were measured in the epicardium, midmyocardium, and endocardium (Fig. 7). The kinetics could be modeled as first-order exponential processes with rate constants of 0.12 min^{-1}, 0.056 min^{-1}, and 0.03 min^{-1}, respectively. As shown in Fig. 7, a slower rate of radical clearance was observed at the location of the endocardium and the left ventricular chamber.

Myocardial Oxygenation. Measurements of myocardial oxygen concentrations were performed from the changes in EPR linewidth, which were observed as a function of the duration of ischemia as was reported previously for simple *in vivo* EPR spectroscopy (4). Examination of the spectral data of the images of the cardiopleged heart showed a gradual decrease in the linewidth at each spatial location (Fig. 8). Over a 60-min duration of ischemia, the linewidth decreased by 0.45 G and approached the linewidth observed in the absence of oxygen. As reported previously, this would correspond to a drop in myocardial oxygen concentration from 625 μM to near 0 μM (4). The linewidth data obtained from the 3D images corresponded closely to those measured from single scan, zero-gradient EPR spectra.

DISCUSSION

After a decade of development and experimentation, the fields of EPR spectroscopy and EPR imaging have advanced to the point of enabling useful physiological and biochemical information to be obtained from living tissues. The development of low-frequency EPR instrumentation at L-band, 1–2 GHz, as well as lumped circuit resonators have made it possible to perform high-quality measurements on these large lossy aqueous samples. Previous studies focused on global measurements of free radical metabolism and measurements of myocardial oxygenation by EPR oximetry techniques (4).

In this manuscript we have reported the development of instrumentation suitable for performing 3D spectral–spatial EPR imaging experiments on large biological samples such as the rat heart. Three-dimensional spectral–spatial images were obtained from isolated perfused rabbit aortas and rat hearts. In the isolated aorta it was observed that spatially and spectrally accurate images could be obtained. In the presence of a paramagnetic contrast agent, the vascular lumen could be clearly resolved. In the isolated rat heart, experiments that imaged the kinetics of radical metabolism during myocardial ischemia were performed. It was observed that there were

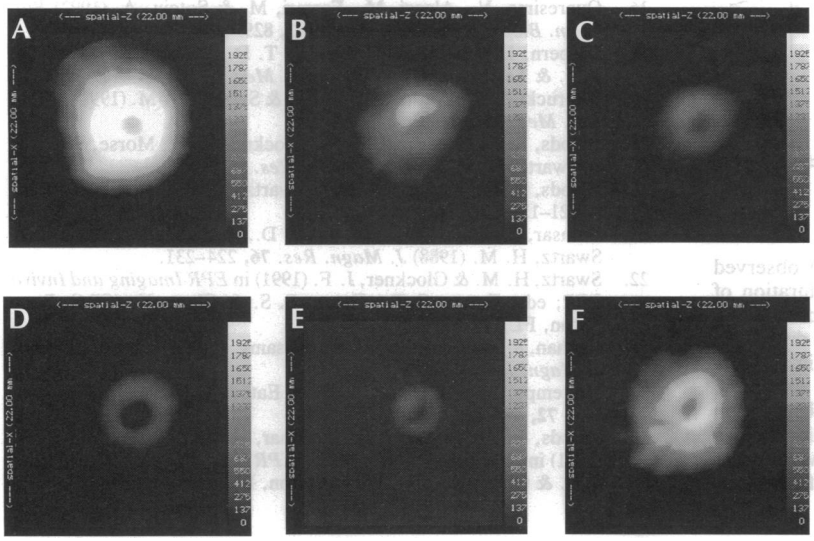

FIG. 6. Series of 2D cross-sectional (22 × 22 mm^2) EPR intensity maps of TEMPO radicals in the heart during normal perfusion (*A*, 0 min), global ischemia (*B*, 12–24 min; *C*, 24–36 min; *D*, 36–48 min; *E*, 50–62 min), and reperfusion (*F*). These images were obtained from a 3D spectral–spatial data reconstructed from 64 projections. Radical clearance of the TEMPO label is observed during ischemia resulting in a decrease in the EPR signal intensity. On reperfusion with TEMPO, the image intensity largely returns.

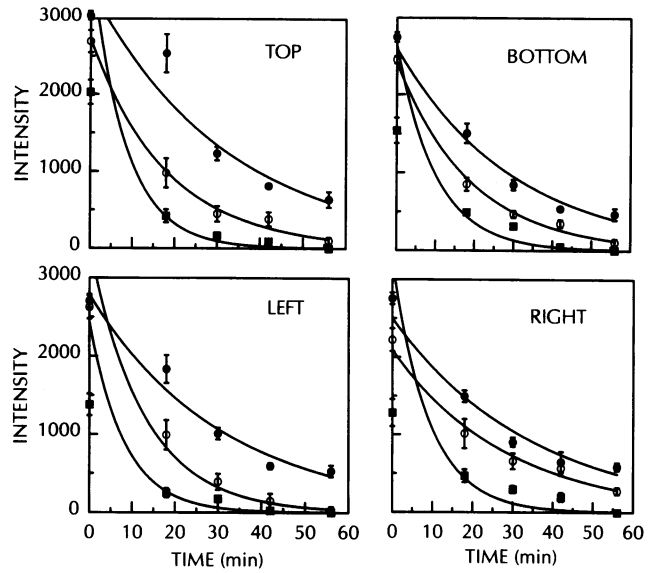

FIG. 7. Graph of the decrease in EPR intensity in the epicardium (■), midmyocardium (○), and endocardium (●) as a function of the duration of ischemia. The Top, Right, Bottom, and Left plots represent 12, 3, 6, and 9 o'clock positions of the heart image, respectively. The solid line through each data set represents a first-order exponential decay curve corresponding to the data set.

spatially defined differences in the rate of radical clearance with the free radical pool present in the area of the endocardium and left ventricular cavity cleared at a slower rate than that within the epi- or midmyocardium. From the spectral data, information was obtained regarding the concentration of oxygen at different spatial locations within the heart.

It has been previously demonstrated that the process of myocardial infarction progresses as a wave front phenomenon from the endocardial surface to the epicardial surface (8, 9). It has been clearly shown that the endocardium is more susceptible to ischemic injury; however, the basis of this phenomenon is unknown. It has been demonstrated that reactive oxygen free radicals are generated in ischemic and reperfused hearts, and it has been suggested that the process

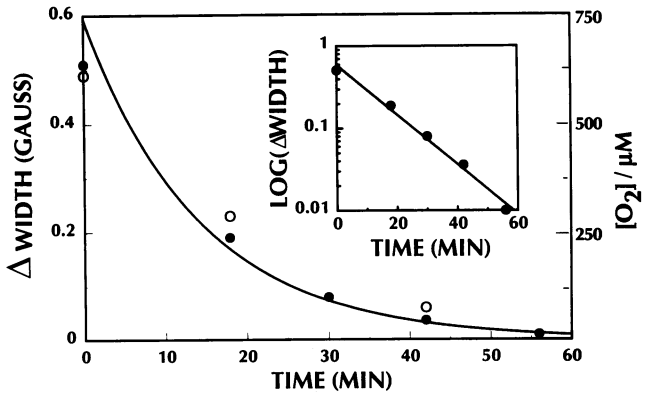

FIG. 8. Graph of the changes in EPR linewidth (●) observed within the heart images (Fig. 6) as a function of the duration of ischemia. The vertical axis shows the value of linewidth broadening caused by molecular oxygen and is calculated as the difference between the observed linewidth from the spectral–spatial image data and the intrinsic width of the signal observed under anaerobic conditions (4). The open circles show the broadening observed in zero-gradient spectra at the corresponding time. The solid line is a first-order exponential fit (k = 0.07 min^{-1}) to the linewidth data. (*Inset*) Semilogarithmic plot of the width as a function of time.

of ischemia could deplete antioxidative defenses and the ability of the heart to metabolize these radicals (8, 9). As such the results obtained in the present study showing a transmural gradient in the rate of myocardial radical clearance with slower clearance in the endocardium could serve to explain the sensitivity of the endocardium to ischemic injury.

We observed that myocardial oxygen concentrations gradually decreased in cardiopleged hearts subjected to room temperature ischemia. In these hearts no evidence of regional or transmural differences in myocardial oxygenation was seen. The rate of decrease in oxygen concentration was observed to be considerably slower than that we have previously reported in noncardiopleged hearts (4). This would be expected since in the cardiopleged hearts contractile function is arrested resulting in a much lower rate of oxygen consumption.

Thus, we have demonstrated that the technique of spectral spatial EPR imaging of free radicals can be performed in living biological organs and tissue. This technique has the ability to address a number of important biomedical problems including localized free radical metabolism and oximetry.

We thank Dr. H. M. Swartz, Dr. R. K. Woods, Dr. G. R. Eaton, Dr. A. Sotgiu, Dr. U. Ewert, and Dr. M. L. Weisfeldt for helpful discussions and advice. This work was supported by National Institutes of Health Grants HL-38324 and HL-17655 and an American Heart Association Established Investigator Award.

1. Froncisz, W. & Hyde, J. S. (1982) *J. Magn. Res.* **47**, 515–521.
2. Lukiewicz, S. J. & Lukiewicz, S. G. (1984) *J. Magn. Res.* **47**, 515–521.
3. Sotgiu, A. (1985) *J. Magn. Res.* **65**, 206–214.
4. Zweier, J. L. & Kuppusamy, P. (1988) *Proc. Natl. Acad. Sci. USA* **85**, 5703–5707.
5. Brivati, J. A., Stevens, A. D. & Symons, M. C. R. (1991) *J. Magn. Res.* **92**, 480–489.
6. Zweier, J. L., Kuppusamy, P. & Lutty, G. A. (1988) *Proc. Natl. Acad. Sci. USA* **85**, 4046–4050.
7. Zweier, J. L., Kuppusamy, P., Williams, R., Rayburn, B. K., Smith, D., Weisfeldt, M. L. & Flaherty, J. T. (1989) *J. Biol. Chem.* **264**, 18890–18895.
8. Reimer, K. A., Lowe, J. E., Rasmussen, M. M. & Jennings, R. B. (1977) *Circulation* **56**, 786–794.
9. Reimer, K. A. & Jennings, R. B. (1979) *Lab. Invest.* **40**, 633–644.
10. Eaton, G. R., Eaton, S. S. & Ohno, K., eds. (1991) *EPR Imaging and Invivo EPR* (CRC, Boca Raton, FL).
11. Ewert, U., Herrling, T. & Schneider, W. (1988) *Magn. Reson. Relat. Phenom. Proc. Congr. Ampere* **30**, 281–294.
12. Berliner, L. J. & Fujii, H. (1985) *Science* **227**, 517.
13. Berliner, L. J., Fujii, H., Wan, X. & Lukiewicz, S. J. (1987) *Magn. Res. Med.* **4**, 380–384.
14. Alecci, M., Colacicchi, S., Indovina, P. L., Momo, F., Pavone, P. & Sotgiu, A. (1990) *Magn. Reson. Imag.* **8**, 59–63.
15. Takeshita, K., Utsumi, H. & Hamada, A. (1991) *Biochem. Biophys. Res. Commun.* **177**, 874–880.
16. Quaresima, V., Alecci, M., Ferrari, M. & Sotgiu, A. (1992) *Biochem. Biophys. Res. Commun.* **183**, 829–835.
17. Halpern, H. J., Peric, M., Nguen, T. D., Bowman, M. K., Lin, Y. J. & Teicher, B. A. (1989) *Phys. Med.* **5**, 147–149.17.
18. Dobrucki, J. W., Sutherland, R. M. & Swartz, H. M. (1991) *Magn. Res. Med.* **19**, 42–55.
19. Woods, R. K., Dobrucki, J. W., Glockner, J. F., Morse, P. D., II & Swartz, H. M. (1989) *J. Magn. Res.* **85**, 50–59.
20. Woods, R. K., Hyslop, W. B. & Swartz, H. M. (1989) *Phys. Med.* **5**, 121–138.
21. Demsar, F., Walczak, T., Morse, P. D., II, Bacic, G., Zolnai, Z. & Swartz, H. M. (1988) *J. Magn. Res.* **76**, 224–231.
22. Swartz, H. M. & Glockner, J. F. (1991) in *EPR Imaging and Invivo EPR*, eds. Eaton, G. R., Eaton, S. S. & Ohno, K. (CRC, Boca Raton, FL), pp. 261–290.
23. Chzhan, M., Shteynbuk, M., Kuppusamy, P. & Zweier, J. L. (1993) *J. Magn. Res.* **105**, 49–53.
24. Maltempo, M. M., Eaton, S. S. & Eaton, G. R. (1987) *J. Magn. Res.* **72**, 449–455.
25. Woods, R. K., Hyslop, W. B., Maar, R. B. & Lauterbur, P. C. (1991) in *EPR Imaging and Invivo EPR*, eds. Eaton, G. R., Eaton, S. S. & Ohno, K. (CRC, Boca Raton, FL), pp. 91–117.